Adaptive Fuzzy-Region-Based Control of Euler–Lagrange Systems With Kinematically Singular Configurations

Hongbo Gao, Wei Bi, Xiaoyu Wu, Zhijun Li, *Senior Member, IEEE*, Zhen Kan, and Yu Kang, *Senior Member, IEEE*

***Abstract*—Singularity issue has long been a concern of the task-space control design for Euler–Lagrange systems. In classical task-space controls, robots are often assumed to operate in the task space, where singularities do not exist. Such an assumption limits their potential applications in various workspaces. To address the potential singularity issue associated with Euler–Lagrange systems, this article proposes an adaptive fuzzy-region-based control for Euler–Lagrange systems with kinematically singular configurations. Singular regions are described by the potential energy function. The proposed controller includes a joint-space control, which is active when the system approaches singular regions, and a task-space control, which is used to track the desired trajectory. Therefore, the system can smoothly transit from singular regions to nonsingular regions or can achieve singularity avoidance during the tracking task. In order to achieve singularity avoidance while reducing control effort, the coefficients of the potential energy function are adjusted dynamically based on the designed fuzzy system. Rigorous analysis shows that singularity issues can be properly handled, and the asymptotic stability of the system is ensured. Experiments are conducted to demonstrate the effectiveness of the proposed controller.**

***Index Terms*—Euler–Lagrange system, fuzzy-region-based control, singularity avoidance, task-space control.**

I. Introduction

EULER–Lagrange systems [1], [2] have been founded in many applications, such as service robots [3], [4], space manipulators [5], unmanned systems [6], [7], etc. In recent years, intensive research attention focuses on the control of Euler–Lagrange systems [8], [9]. Various methods in the literature have been proposed to handle the tracking problem, such as disturbance observer [10], sliding-mode approach [11], and expanded proportional–integral controller [12]. Extensions to deal with unknown parametric uncertainties are introduced in [13], where an adaptive control scheme is presented to synchronize nonidentical Euler–Lagrange systems with communication latency.

Many studies have been proposed to address parametric uncertainties, coupled dynamics, and nonlinear physical limits of actuators in Euler–Lagrange systems [14]–[16]. In [17], an adaptive control method using feedback linearization for the multiple-input multiple-output robot system with input parametric uncertainties was proposed. In [18], the vibration control and the trajectory tracking control of a Euler–Lagrange system with input constraints were developed, where hyperbolic tangent functions and saturation functions were employed to handle input constraints. Although the tracking control of Euler–Lagrange systems has been extensively studied, kinematically singular configurations existing in Euler–Lagrange systems have not been fully considered in the literature. Therefore, this article is practically motivated to address the issue of kinematically singular configurations when controlling Euler–Lagrange systems.

In previous studies, singularity avoidance or singularity robust methods were only considered in robotic systems [19], [20]. At a singular configuration, the inverse kinematic problem cannot be solved due to infinite joint velocities. Approaching a configuration close to a singularity may result in high joint speeds, which is dangerous to human operators. In order to handle the singularity problem, a special inverse Jacobian matrix was developed in [19], which used the damped least squares to generate a proximate motion trajectory when the robotic end-effector is near singular configurations. In [22], a method adopting the Jacobian transpose rather than the inverse Jacobian matrix was introduced to avoid robotic system instabilities. Based on joint torque optimization, a new robust controller was proposed in [21] to handle robot kinematic singularities. In this method, the damped least-squares inverse of the Jacobian-inertia product was used to control the end-effector's motions in the neighborhood of singular regions. The damping factor was then used as a function of the generalized dynamic operation measure to reduce the robotic end-effector acceleration error caused by

Manuscript received November 11, 2019; revised March 18, 2020; accepted May 7, 2020. Date of publication May 15, 2020; date of current version August 4, 2021. This work was supported in part by the National Natural Science Foundation of China under Grant 61751310 and Grant U1913601, in part by the National Key Research and Development Program of China under Grant 2017YFB1302302, Grant 2018YFC2001600, and Grant 2018YFC2001602, in part by the Anhui Science and Technology Major Program under Grant 17030901029, in part by the Fundamental Research Funds for the Central Universities, in part by the Science and Technology Innovation Planning Project of Ministry of Education of China, and in part by the Key Laboratory of Advanced Perception and Intelligent Control of High-end Equipment of Ministry of Education (Anhui Polytechnic University, Wuhu, China, 241000) under Grants GDSC202001 and GDSC202007. *(Corresponding author: Zhijun Li.)*

The authors are with the Department of Automation, University of Science and Technology of China, Hefei 230060, China (e-mail: ghb48@ustc.edu.cn; biw@mail.ustc.edu.cn; xiaoyuw@mail.ustc.edu.cn; zjli@ieee.org; zhen-kan@uiowa.edu; kangduyu@ustc.edu.cn).

Color versions of one or more of the figures in this article are available online at https://ieeexplore.ieee.org.

Digital Object Identifier 10.1109/TFUZZ.2020.2994991

damping. In [24], singular configurations were avoided using inverse kinematic solutions to increase robot manipulability. In [25], a redundancy control scheme was introduced with task-priority tactics, where the system's tracking task has higher priority than singularity avoidance. In [26], a fuzzy robot motion planning framework was introduced to handle singularity issues in inverse kinematics. The position of the redundant robotic end-effector was obtained through a fuzzy motion planning mapping algorithm, and the errors in singular configurations were approximately reduced to zero. However, it is difficult to employ the Jacobian transpose or the damped inverse Jacobian to testify the stability of the closed-loop system, and redundancy approaches are only applicable to the redundant robot, which has more freedom of motion than the degree of freedom (DoF) required for the task. In addition, these methods are only applicable to robotic systems extended to Euler–Lagrange systems.

In order to avoid singularities in the Euler–Lagrange systems with dynamics uncertainties, an adaptive controller with unit quaternion representation was proposed in [27], in which the four-parameter representation was used to parameterize the orientations of the system's end-effector to facilitate singularity avoidance. However, this method is only applicable for singularities in the joint space. In [28], a singularity-robust tracking controller was developed to enable the system to leave the singular position or enter the singular position. The controller included a joint-space controller and a task-space tracking controller. Although the task-space tracking controller was locally effective in a limited task space where singular configurations do not exist, the stability of the closed-loop system has not been systemically investigated. A regional feedback approach was presented in [29], which systemically addressed the stability of the system with singularities. In [30], by using the singular region function and the potential energy function, system can transit steadily from the singular region to the nonsingular region. Unfortunately, coefficients of the potential energy function in previous methods are fixed, which provides less flexibility to tune the system performance and thus leads to more control effort to force the robot to leave singular configurations. Specifically, traditional approaches based on fixed coefficients mainly depend on the positions of the system, without considering its motion direction. For instance, when the system is close to the singular region and moves away from the singular region, less control effort is required for singularity avoidance, compared with the case that the system moves toward the singular region. Therefore, this article is motivated to develop a potential energy function, in which the coefficients are adjustable to account for both position and velocity of the system so that singularity avoidance and task tracking can be achieved with less control effort.

In this article, an adaptive fuzzy-region-based control is presented for Euler–Lagrange systems with kinematically singular configurations. The singular region is defined in joint space and task space using potential energy functions, in which the gain coefficients are adjustable based on the characteristics of the fuzzy system. In previous studies, fuzzy potential energy (FPE) was proposed to build a map to facilitate path planning for mobile robots [31]. In [32], a fuzzy-based potential field method was presented for path planning of the mobile robot in an environment with dynamic and static obstacles. In [33], an enhanced fuzzy-behavior-based framework is proposed. Fuzzy logic was used to achieve individual robot behaviors, such as selecting roles, robot perception, and robot decision making in a multiagent environment. In [34], a fuzzy adaptive tracking controller for mobile robots was proposed, in which the adaptive observers with the parameter fuzzy adaptation laws were used to estimate the dynamic and kinematic disturbances of the system. Compared with traditional approaches, fuzzy control is more robust in the sense that it does not require accurate system models. In this article, based on the fuzzy system, an adaptive fuzzy-region-based control is proposed for Euler–Lagrange systems to avoid singularities, in which control coefficients are adjustable to account for both position and velocity of the system in order to optimize the performance of trajectory tracking and singularity avoidance. Therefore, the designed controller can not only extend singularity avoidance to the Euler–Lagrange system with kinematics singular configuration, which has not been largely studied in the literature, but also reduce the control effort due to the optimization of control parameters. Then, we prove that the developed control guarantees the asymptotic stability of the Euler–Lagrange system while avoiding singular regions during the tracking task or starting from a singular position. The effectiveness of the proposed control method has been validated by the experiments with a two-DoF robotic manipulator.

II. System Dynamics

The dynamics of an n-DoF Euler–Lagrange system can be described as

$$M(q)\ddot{q} + C(q,\dot{q})\dot{q} + G(q) = \tau + \tau_e \tag{1}$$

where q is the joint variable of the system, $M(q) \in \Re^{n\times n}$ is the inertia matrix, which is symmetric and positive definite, $C(q,\dot{q}) \in \Re^{n\times n}$ represents the centrifugal Coriolis torques, $G(q) \in \Re^n$ denotes a vector of gravitational torque, $\tau \in \Re^n$ represents a vector of control input, and $\tau_e \in \Re^n$ denotes the torque exerted by environment. The centrifugal Coriolis torques $C(q,\dot{q})$ satisfy $\dot{M}(q) = C(q,\dot{q}) + C(q,\dot{q})^T$, which indicates that $\dot{M}(q) - 2C(q,\dot{q})$ is skew symmetric [35]. The dynamics model in (1) exhibits parametric uncertainties. Considering the friction and oscillation of the system, since fuzzy control is robust to noisy data, we adopt a fuzzy approximator to compensate for the system uncertainties [36].

Property 1: Suppose that $f(x)$ is an unknown nonlinear function, and let $\hat{f}(x|\theta_f)$ denote the approximate of $f(x)$. The fuzzy system $\hat{f}(x|\theta_f)$ is constructed as follows: 1) for each state variable $x_i \in x$, define p_i fuzzy sets $A_i^{l_i}(l_i = 1, 2, \ldots, p_i)$; and 2) the fuzzy system $\hat{f}(x|\theta_f)$ is constructed by $\prod_{i=1}^{n} p_i$ fuzzy rules as follows: *IF* x_1 *is* $A_1^{l_1}$ *and ... and* x_n *is* $A_n^{l_n}$, *THEN* $\hat{f}$ *is* $E^{l_1\ldots l_n}$. $E^{l_1\ldots l_n}$ is the output fuzzy set.

Property 2: Using the product inference engine, single-valued fuzzy, and the center of gravity (COG) defuzzification, the single fuzzy controller can be described as

$$\hat{f}(x|\theta_f) = \frac{\sum_{l_1=1}^{p_1}\cdots\sum_{l_n=1}^{p_n}\overline{y}_f^{l_1\ldots l_n}\left(\prod_{i=1}^{n}\mu_{A_i^{l_i}}(x_i)\right)}{\sum_{l_1=1}^{p_1}\cdots\sum_{l_n=1}^{p_n}\left(\prod_{i=1}^{n}\mu_{A_i^{l_i}}(x_i)\right)} \tag{2}$$

where $\mu_{A_i^{l_i}}(x_i)$ is the membership function of x_i, and $\overline{y}_f^{l_1 \ldots l_n}$ is the free parameter used in set $\theta_f \in R^{\prod_{i=1}^{n} p_i}$. Define the fuzzy basis function as

$$\xi_{l_1 \ldots l_n}(x) = \frac{\prod_{i=1}^{n} \mu_{A_i^{l_i}}(x_i)}{\sum_{l_1=1}^{p_1} \cdots \sum_{l_n=1}^{p_n} \left(\prod_{i=1}^{n} \mu_{A_i^{l_i}}(x_i) \right)}. \quad (3)$$

Using $\xi(x)$, which is a $\prod_{i=1}^{n} p_i$-dimensional vector, (2) is rewritten as

$$\hat{f}(x|\theta_f) = \theta_f^T \xi(x). \quad (4)$$

III. Singular Regions and FPE Function

A. Joint-Space Singular Regions

Singularities of the Euler–Lagrange systems can be classified as external singularities and internal singularities. The external singularities appear on the boundary of the system's external task space, while the internal singularities consist of interior singularities and internal boundary singularities.

The region around a singular point is defined as the singular region in joint space. External singular regions are described as

$$f_E(q) = [f_{E1}(q), f_{E2}(q), \ldots, f_{En_e}(q)] \geq 0 \quad (5)$$

where n_e is the number of external singular configurations in joint space.

Similarly, internal singular regions are defined as

$$f_I(q) = [f_{I1}(q), f_{I2}(q), \ldots, f_{In_i}(q)] \geq 0 \quad (6)$$

where n_i is the number of internal singular configurations.

The modality of singular region functions is related to the types of Euler–Lagrange systems. Particularly, a two-DoF planar manipulator whose Jacobian matrix $J(q)$ is described in (7) is taken as an example

$$J(q) = \begin{bmatrix} -l_1 \sin(q_1) - l_2 \sin(q_1 + q_2) & -l_2 \sin(q_1 + q_2) \\ l_1 \cos(q_1) + l_2 \cos(q_1 + q_2) & l_2 \cos(q_1 + q_2) \end{bmatrix}. \quad (7)$$

The Jacobian matrix is singular when

$$\det[J(q)] = l_1 l_2 \sin(q_2) = 0 \quad (8)$$

where l_1 and l_2 are the lengths of the planar manipulator, and q_2 is the second joint angle. Therefore, singular configurations of planar manipulator occur when $q_2 = 0$ and $q_2 = \pi$.

The external boundary singularity corresponds to the joint angle $q_2 = 0$, and external singular regions in the joint space are a set of points q satisfying

$$f_E(q) = \frac{1}{d^2(q_2, 0)} - \frac{1}{b_E^2} \geq 0 \quad (9)$$

where $d(q_2, 0)$ is the distance between the joint q_2 and the singularity 0, and $b_E > 0$ denotes the region radius.

The internal boundary singularity corresponds to the joint angle $q_2 = \pi$, and internal singular regions in the joint space are described as

$$f_I(q) = \frac{1}{d^2(q_2, \pi)} - \frac{1}{b_I^2} \geq 0 \quad (10)$$

where $d(q_2, \pi)$ is the distance between the joint q_2 and the singularity π, and $b_I > 0$ denotes the region radius.

After defining singular region functions for the joint space in (9) and (10), the potential energy function based on the region function is developed as

$$P_{Ei}(q) = \frac{\beta_i}{N} \max(f_{Ei}, 0)^N \quad (11)$$

$$P_{Ii}(q) = \frac{\eta_i}{N} \max(f_{Ii}, 0)^N \quad (12)$$

where $P_{Ei}(q)$ denotes potential energy functions for external singular regions and $P_{Ii}(q)$ denotes potential energy functions for internal singular regions. β_i and η_i are their coefficients, respectively. In order to ensure that the potential energy is nonnegative, the order of region function N should be defined as an even number with $N \geq 2$. That means the potential energy of the Euler–Lagrange system is defined for the inside and outside of the region, respectively. The gradient of potential energy functions can be used in system control, with parameters β_i and η_i being the system control gains. When the system is inside the singular regions, the gradient should be nonzero so that the potential field drives the system to leave the singular region. When the system is outside the singular regions, the gradient should decrease to zero. The potential energy is also smooth during the transitions between the inside and outside of the singular regions, so the system can avoid hard switching issues.

B. FPE Function

To avoid singularities effectively, the coefficients of the potential energy function β_i and η_i can be adjusted according to the current angle q_i and its angular velocity $\dot{q}_i$. This method can optimize the energy consumed and reduce the required control effort to force the system to leave the singular configurations. In this article, we propose a fuzzy controller, which consists of double input and single output using a fuzzy control method, in order to construct an adjustable potential energy function.

For example, we consider a two-DoF planar robotic manipulator. The double inputs of the fuzzy controller are q_2 and $\dot{q}_2$, and the single output is β_2 or η_2. The relationship between the singularity and the joint can be determined by the position of the joint and the direction of the joint movement. The double input and single output adopt continuous theory field and use a simple linear method. For easy use and effectiveness, we choose triangular membership functions, which are defined as

$$\text{Triangle}(\nu : a, b, c) = \begin{cases} 0, & \nu < a \\ \frac{\nu - a}{b - a}, & a \leq \nu \leq b \\ \frac{c - \nu}{c - b}, & b \leq \nu \leq c \\ 0, & \nu > c \end{cases} \quad (13)$$

where ν is the input and the parameters are $a, b,$ and c with $a < b < c$.

The theory field $(-\pi, \pi)$ of joint angle q_2 can be segmented into seven linguistic terms: NB (negative big), NM (negative middle), NS (negative small), ZO (zero), PS (positive small), PM (positive middle), and PB (positive big); the theory field $(-1, 1)$ of joint velocity $\dot{q}_2$ can be divided into five linguistic

TABLE I
FUZZY RULES 1 FOR EXTERNAL SINGULARITY

$\dot{q}_2$	q_2						
	NB	NM	NS	ZO	PS	PM	PB
NH	NA	NA	NA	BA	MA	SA	NA
NL	NA	NA	NA	MA	MA	NA	NA
ZO	NA	NA	SA	MA	SA	NA	NA
PL	NA	NA	MA	MA	NA	NA	NA
PH	NA	SA	MA	BA	NA	NA	NA

TABLE II
FUZZY RULES 2 FOR INTERNAL SINGULARITY

$\dot{q}_2$	q_2						
	NB	NM	NS	ZO	PS	PM	PB
NH	BA	MA	NA	NA	NA	NA	SA
NL	BA	SA	NA	NA	NA	NA	SA
ZO	MA	NA	NA	NA	NA	NA	MA
PL	SA	NA	NA	NA	NA	SA	BA
PH	SA	NA	NA	NA	NA	MA	BA

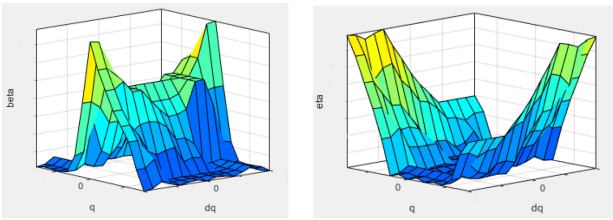

(a) (b)

Fig. 1. Input and output variation curved surface of the fuzzy system. (a) External singularity. (b) Internal singularity.

terms: NH (negative high), NL (negative low), ZO (zero), PL (positive low), and PH (positive high). The theory field $(1, 10)$ of coefficients β_2 and η_2 can be segmented into four linguistic terms: NA (none affect), SA (small affect), MA (middle affect), and BA (big affect). Fuzzy rules are detailed in Tables I and II. We use the center of area for defuzzification described in (14) to calculate the output. The input and output variation curved surface is detailed in Fig. 1. The COG defuzzification method is defined as

$$y = \frac{\sum_{i=1}^{j} \mu_A(y_i) y_i}{\sum_{i=1}^{j} \mu_{A_i}(y_i)} \tag{14}$$

where j is the number of subfuzzy sets chosen, $\mu_A(y_i)$ denotes the degree of membership function A_i, and y_i denotes the value at the base center of the corresponding membership function.

Property 3: FPE functions P_{E2} in (11) and P_{I2} in (12) satisfy the following properties.

1) $P_{E2} = P_{I2} = 0$, when $d(q_2, 0) \geq b_E$ and $d(q_2, \pi) \geq b_I$.
2) $P_{E2} > 0$ and $P_{I2} > 0$, when $d(q_2, 0) < b_E$ and $d(q_2, \pi) < b_I$.

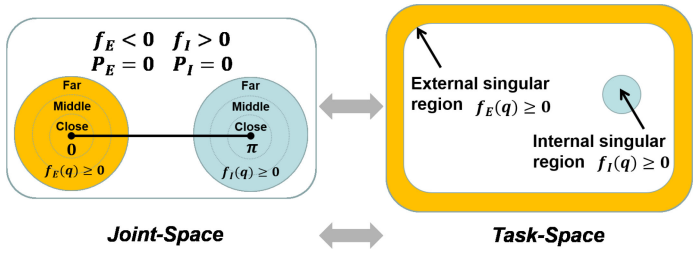

Fig. 2. Singular regions.

3) The values of P_{E2} and P_{I2} depend on the magnitude and direction of q_2 and $\dot{q}_2$. When q_2 is far from the singularity and $\dot{q}_2$ is moving away from singularity, the influence of β_2 or η_2 is smaller, i.e., the potential energy P_{E2} or P_{I2} is smaller. On the contrary, when q_2 is close to the singularity and $\dot{q}_2$ is moving toward singularity, the influence of β_2 or η_2 is greater and the potential energy P_{E2} or P_{I2} is larger, resulting in a larger control effort. It should be emphasized that when q_2 is close to the singular regions, with the direction of its motion $\dot{q}_2$ moving away from the singular regions, the system does not require extra effort to keep it away from the singular region, so the influence of β_2 or η_2 should be decreased to avoid unnecessary effort.

Potential energy functions in (11) and (12) on singular regions in the joint space are illustrated in Fig. 2. Then, the total potential energy can be introduced as

$$\begin{aligned} P_S(q) &= \alpha_s \left(\sum_{i=1}^{n_e} P_{Ei} + \sum_{i=1}^{n_i} P_{Ii} \right) \\ &= \alpha_s \left(\sum_{i=1}^{n_e} \frac{\beta_i}{N} [\max(f_{Ei}, 0)]^N + \sum_{i=1}^{n_i} \frac{\eta_i}{N} [\max(f_{Ii}, 0)]^N \right) \end{aligned} \tag{15}$$

where $\alpha_s > 0$ is a constant coefficient and $N \geq 2$ is an even number. Therefore, the potential energy is lower bounded by zero. The illustration of its potential energy $P_s(q)$ is shown in Fig. 4. Whenever the system enters the singular regions, its potential energy is nonzero, and the gradient is also nonzero such that potential energy field drives the system away from the singular regions. However, the potential energy reduces to zero when the system leaves the singular regions.

C. Task-Prioritized Region and FPE Function

The singular regions corresponding to the joint space could also be defined in the task space. Because the inverse Jacobian matrix does not exist at the singular configurations, the subspaces where the Euler–Lagrange system cannot use task-space feedback are defined as task-space singular regions. First, the task-prioritized regions excluding all external singular positions are specified as a set of points x satisfying

$$f_E(\Delta x) = \frac{(x_1 - x_{d1})^{N_e}}{(x_{b1} - x_{d1})^{N_e}} + \cdots + \frac{(x_n - x_{dn})^{N_e}}{(x_{bn} - x_{dn})^{N_e}} - 1 \leq 0 \tag{16}$$

where $x_d = [x_{d1}, \ldots, x_{dn}]^T$ denotes the desired trajectory, $\Delta x = x - x_d$, $x_b = [x_{b1}, \ldots, x_{bn}]^T$ denotes the boundary positions of the task-prioritized regions, and $x = [x_1, \ldots, x_n]^T$ denotes the actual trajectory. N_e is the order of task-prioritized region function. It should be emphasized that the task-prioritized region is designed to ensure the convergence of the system to the desired position x_d. The potential energy function of the task-prioritized region is defined as

$$P_E(x) = \frac{k_p}{N}\{1 - [\min(0, f_E(\Delta x))]^N\} \tag{17}$$

where k_p is an adjustable positive coefficient. According to the potential energy function (17), $P_E(x)$ is nonnegative and differentiable. According to (17), the potential energy is constant when the system is outside the task-prioritized region, so the gradient of potential field is zero. $P_E(\Delta x)$ increases as the distance $\|x - x_d\|$ increases. Because the potential energy reaches the minimum value where the system is at the desired position, the potential field will drive the system to track the desired position x_d when the system is inside the task-prioritized region.

Because the internal singularities appear in the interior of the workspace, the internal task-space singular regions that surround the internal singular configurations are described as

$$\begin{aligned} f_I(x) &= [f_{I1}(x), \ldots, f_{In_i}(x)] \\ f_{Ii}(x) &= \frac{(x_1 - x_{ri1})^{N_i}}{a_i^{N_i}} + \cdots + \frac{(x_n - x_{rin})^{N_i}}{a_i^{N_i}} - 1 \le 0 \end{aligned} \tag{18}$$

where $x_r = [x_{r1}, \ldots, x_{rn}]^T$ represents static reference points corresponding to the internal singularities in joint space, a_i represents positive constants denoting the range of regions, and N_i is the order of region function.

Then, the transition region is designed as

$$f_{IRi}(x) = \frac{(x_1 - x_{ri1})^{N_i}}{a_{ri}^{N_i}} + \cdots + \frac{(x_n - x_{rin})^{N_i}}{a_{ri}^{N_i}} - 1 \le 0 \tag{19}$$

where a_{ri} represents the radius of the transition region such that $a_{ri} > a_i$. The transition region is used to ensure smooth transition between task-prioritized regions and internal singular regions in task space.

According to the internal task-space singular regions and transition regions, the potential energy function $P_{Ii}(x)$ can be defined as

$$\begin{aligned} P_{Ii}(x) = \frac{k_{xi}}{N^2}\Big\{\min\Big[0, [\min(0, f_{IRi}(x))]^N \\ - \left(\frac{a_i^{N_i} - a_{ri}^{N_i}}{a_{ri}^{N_i}}\right)^N\Big]\Big\}^N \end{aligned} \tag{20}$$

where k_{xi} is an adjustable positive coefficient.

Inspired by the fuzzy system, the fuzzy set theory can be used to optimize the coefficients of potential energy functions $P_E(x)$ and $P_{Ii}(x)$, so that the task can be achieved more efficiently and effectively while reducing the required control effort. The values of k_p depend on the system position error $x - x_d$ and speed error $\dot{x} - \dot{x}_d$, while k_{xi} is dependent on $x - x_r$ and $\dot{x} - \dot{x}_r$ in the task space. All variables employ continuous theory field and use a simple linear method. Similarly, Gaussian membership functions are used to specify fuzzy sets, since they have terse notation, and smooth curves are nonzero at all points. Therefore, we choose the Gaussian function described in (21) as the membership grade function for all variables. The Gaussian function based on two parameters σ_i and ι_i is defined as

$$\text{Gaussian}(\nu_i : \sigma_i, \iota_i) = \exp\left[-\left(\frac{\nu_i - \iota_i}{2\sigma_i}\right)^2\right]. \tag{21}$$

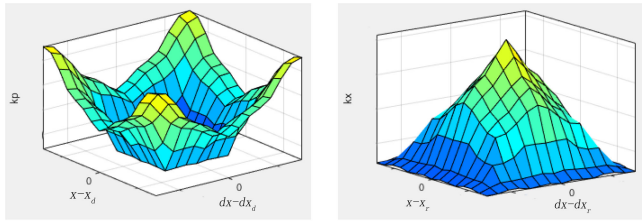

(a) (b)

Fig. 3. Input and output variation curved surface of the fuzzy system. (a) Task-prioritized region. (b) Internal task-space singular region.

For example, consider a two-DoF planar manipulator, the theory field $(-0.02, 0.02)$ of the end-effector's position error $x - x_d$ and speed error $\dot{x} - \dot{x}_d$, and the theory field $(-0.1, 0.1)$ of the end-effector's position error $x - x_r$ and speed error $\dot{x} - \dot{x}_r$ are split into five linguistic terms: NB (negative big), NS (negative small), ZO (zero), PS (positive small), and PB (positive big). The theory field (1,10) of the coefficients of potential energy functions k_p and k_{x2} is split into four linguistic terms: NA (none affect), SA (small affect), MA (middle affect), and BA (big affect). The fuzzy rules of two fuzzy controllers are similar to the above mentioned and are not described in detail here. Then, the input and output variation curved surfaces are detailed in Fig. 3.

The potential energy of task space $P_x(x)$ is the combinations of $P_E(x)$ and $P_{Ii}(x)$

$$\begin{aligned} P_x(x) = \alpha_x \Bigg\{ P_E(x) \prod_{i=0}^{n_i} P_{Ii}(x) - \sum_{i=1}^{n_i} P_{Ii}(x) \\ + \frac{k_{xi}}{N} \sum_{i=1}^{n_i} \left(\frac{a_i^{N_i} - a_{ri}^{N_i}}{a_{ri}^{N_i}}\right)^N \Bigg\} \end{aligned} \tag{22}$$

where $\alpha_x > 0$ is a constant coefficient and $N \ge 2$ is an even number. Therefore, $P_x(x)$ is smooth and lower bounded by zero. Considering a task space with an internal singular region and an external singular region [recalling Fig. 2(a)]. The illustration of its potential energy $P_x(x)$ is shown in Fig. 5. According to Fig. 5, the desired position x_d corresponds to the nadir of $P_x(x)$, and the top profile of $P_x(x)$ corresponds to the task-prioritized region $f_E(x)$. Since x_d is time varying, the top profile and nadir of $P_x(x)$ are time varying.

When the system is outside the task-prioritized region $f_E(x)$ or inside the internal task-space singular region $f_I(x)$, $P_x(x)$ is constant, so the gradient of $P_x(x)$ is zero. When the system

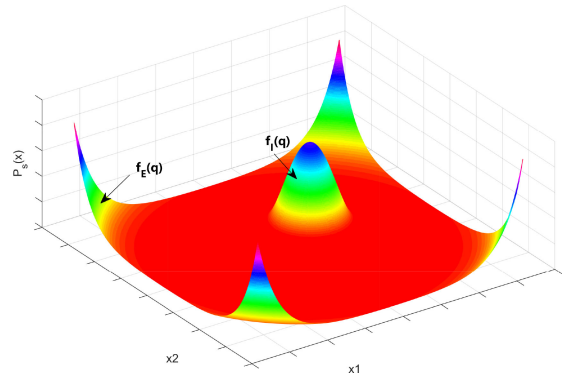

Fig. 4. Potential energy in joint space.

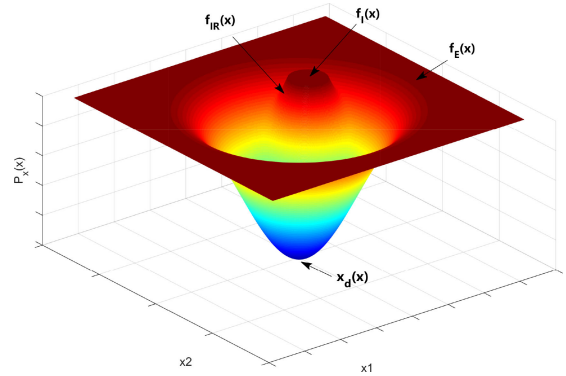

Fig. 5. Potential energy in task space.

is inside the task-prioritized region $f_E(x)$ but outside the internal task-space singular region $f_I(x)$, the potential energy field drives the system to track the desired position x_d because the potential energy function reaches the minimum value when the system is at the desired position.

IV. Controller Design and Stability Analysis

According to (1), the dynamics of the Euler–Lagrange systems are rewritten as

$$\dot{x}_1 = x_2 \tag{23}$$

$$\dot{x}_2 = M^{-1}[\tau + \tau_e - G - Cx_2] \tag{24}$$

where $x_1 = [q_1, q_2, q_3, ..., q_n]^T$ and $x_2 = [\dot{q}_1, \dot{q}_2, \dot{q}_3, \ldots, \dot{q}_n]^T$. Given the desired joint angles q_d, the errors z_1 and z_2 are defined as

$$z_1 = x_1 - q_d \tag{25}$$

$$z_2 = x_2 - \alpha_1 \tag{26}$$

where α_1 is the virtual control to z_2.

Consider the Lyapunov function candidate $V_1 = P_s + P_x$, where P_s and P_x are defined in (15) and (22). First, taking partial derivative of $P_s(q)$ with respect to q, we have

$$\left(\frac{\partial P_s(q)}{\partial q}\right)^T = \alpha_s \sum_{i=1}^{n_e} \beta_i \left[\max(0, f_{Ei}(q))\right]^{N-1} \left(\frac{\partial f_{Ei}(q)}{\partial q}\right)^T + \alpha_s \sum_{i=1}^{n_i} \eta_i [\max(0, f_{Ii}(q))]^{N-1} \left(\frac{\partial f_{Ii}(q)}{\partial q}\right)^T = \Delta\varepsilon_q \tag{27}$$

where $\Delta\varepsilon_q$ is the system control component when the system is near or inside the external or internal singularities in task space, which forces the system to avoid the singular configurations. It is worth noting that the two items on the right-hand side of (27) will not coexist. Specifically, if the system enters the external singular regions, the first term is nonzero, while the second term is zero, i.e., $\Delta\varepsilon_q = \alpha_s \sum_{i=1}^{n_e} \beta_i [\max(0, f_{Ei}(q))]^{N-1} (\frac{\partial f_{Ei}(q)}{\partial q})^T$. If the system enters the internal singular regions, the second term is nonzero, while the first term is zero, i.e., $\Delta\varepsilon_q = \alpha_s \sum_{i=1}^{n_i} \eta_i [\max(0, f_{Ii}(q))]^{N-1} (\frac{\partial f_{Ii}(q)}{\partial q})^T$. When the system is outside the external and internal singular regions simultaneously, $\Delta\varepsilon_q = 0$.

Similarly, taking partial derivative of $P_x(x)$ in (22) with respect to x, we have

$$\left(\frac{\partial P_x(x)}{\partial x}\right)^T = \alpha_x \left(\frac{\partial P_E(x)}{\partial \Delta x}\right)^T \prod_{i=0}^{n_i} P_{Ii}(x) - \sum_{i=1}^{n_i} \left(\frac{\partial P_{Ii}(x)}{\partial x}\right)^T + P_E(x) \sum_{i=1}^{n_i} \left[\left(\frac{\partial P_{Ii}(x)}{\partial x}\right)^T \prod_{i \neq j}^{n_i} P_{ji}(x)\right] = \Delta\varepsilon_x \tag{28}$$

where $\frac{\partial P_E(x)}{\partial \Delta x}$ and $\frac{\partial P_I(x)}{\partial x}$ can be obtained from (29) and (30) as

$$\left(\frac{\partial P_E(x)}{\partial \Delta x}\right)^T = k_p [\max(0, f_E(\Delta x))]^{N-1} \left(\frac{\partial f_E(\Delta x)}{\partial \Delta x}\right)^T \tag{29}$$

$$\left(\frac{\partial P_{Ii}(x)}{\partial x}\right)^T = [\min(0, f_{IRi}(x))]^{N-1} \left(\frac{\partial f_{Ii}(x)}{\partial x}\right)^T \times k_{xi} \left\{\min\left[0, \min(0, f_{IRi})^N - \left(\frac{a_i^{N_i} - a_{ri}^{N_i}}{a_{ri}^{N_i}}\right)^N\right]\right\}^{N-1}. \tag{30}$$

$\Delta\varepsilon_x$ is the system control component when the system is outside external or internal singularities in task space, which forces the system to track the desired positions. When system's position error $\Delta x = 0$, $\frac{\partial P_E(x)}{\partial \Delta x} = 0$, $P_E(x)$ and $\frac{\partial P_I(x)}{\partial x}$ also decrease to zero because the system leaves the internal singular regions at this time. Hence, $\Delta\varepsilon_x$ decreases to zero if $\Delta x = 0$ according to (28). In order to ensure $\Delta\varepsilon_q$ and $\Delta\varepsilon_x$ not to decrease to zero simultaneously, regions of both $\Delta\varepsilon_q$ and $\Delta\varepsilon_x$ should have a small overlap. According to $\Delta\varepsilon_q$ and $\Delta\varepsilon_x$, it should be emphasized that the proposed method is better than the conventional task-space feedback controller. It can be understood by the following explanation: when the system is near the singular configurations, $J(q)$ in (7) is not full rank, so the control input could be unbounded. However, in the proposed method, $\Delta\varepsilon_q$, which does not involve $J(q)$, operates when the system is near the singular configurations, so system control input is bounded.

Next, combining (27) and (28), the time derivative of V_1 is

$$\begin{aligned}\dot{V}_1 &= \Delta\varepsilon_q^T\dot{q} + \Delta\varepsilon_x^T\Delta\dot{x} \\ &= \Delta\varepsilon_q^T(\dot{z}_1 + \dot{q}_d) + \Delta\varepsilon_x^T J(q)\dot{z}_1 \\ &= (\Delta\varepsilon_q^T + \Delta\varepsilon_x^T J(q))\dot{z}_1 + \Delta\varepsilon_q^T\dot{q}_d \end{aligned} \tag{31}$$

where

$$\dot{z}_1 = \dot{x}_1 - \dot{q}_d = z_2 + \alpha_1 - \dot{q}_d. \tag{32}$$

The virtual control law is designed as

$$\alpha_1 = \frac{\Delta\varepsilon_x^T J(q)\dot{q}_d}{\Delta\varepsilon_q^T + \Delta\varepsilon_x^T J(q)} - A_1 \tag{33}$$

where A_1 is defined as

$$A_1 = \Delta\varepsilon_q + J^T(q)\Delta\varepsilon_x. \tag{34}$$

Substituting (33)–(34) into (31) yields

$$\begin{aligned}\dot{V}_1 = &-(\Delta\varepsilon_q^T + \Delta\varepsilon_x^T J(q))(\Delta\varepsilon_q + J^T(q)\Delta\varepsilon_x) \\ &+ (\Delta\varepsilon_q^T + \Delta\varepsilon_x^T J(q))z_2. \end{aligned} \tag{35}$$

We know that regardless of q, the first term of (35) is negative. Consider the following Lyapunov function:

$$V_2 = V_1 + \frac{1}{2}z_2^T M z_2 \tag{36}$$

and its time derivative is

$$\dot{V}_2 = \dot{V}_1 + z_2^T M\dot{z}_2 + \frac{1}{2}z_2^T\dot{M}z_2 \tag{37}$$

where

$$\begin{aligned}\dot{z}_2 &= \dot{x}_2 - \dot{\alpha}_1 \\ &= M^{-1}[\tau + \tau_e - G - Cx_2] - \dot{\alpha}_1. \end{aligned} \tag{38}$$

Substituting (35) and (38) into (37) yields

$$\begin{aligned}\dot{V}_2 = &-(\Delta\varepsilon_q^T + \Delta\varepsilon_x^T J(q))(\Delta\varepsilon_q + J^T(q)\Delta\varepsilon_x) \\ &+ (\Delta\varepsilon_q^T + \Delta\varepsilon_x^T J(q))z_2 \\ &+ z_2^T\left(\tau + \tau_e - G - C\alpha_1 - M\dot{\alpha}_1\right). \end{aligned} \tag{39}$$

Based on the above analysis, the controller is designed as

$$\begin{aligned}\tau = &-(\Delta\varepsilon_q + J^T(q)\Delta\varepsilon_x) - K_2 z_2 \\ &+ G + C\alpha_1 + M\dot{\alpha}_1 - \tau_e. \end{aligned} \tag{40}$$

Since the exact model of G, C, and M is not available, we propose the feedforward fuzzy approximator shown in Properties 1 and 2 to estimate the unknown components as

$$\Theta^{*T}\xi = M\dot{\alpha}_1 + C\alpha_1 + G + w \tag{41}$$

with the fuzzy approximation error w satisfying $|w_i| \le w_{Mi}$, where w_{Mi} is a predefined bound. Choose $\Lambda = \mathrm{diag}[\mathrm{w_{M1}}, \mathrm{w_{M2}}]$.

Therefore, τ in (40) can be rewritten as

$$\begin{aligned}\tau = &-(\Delta\varepsilon_q + J^T(q)\Delta\varepsilon_x) - K_2 z_2 \\ &+ \hat{\Theta}^T\xi - \Lambda\mathrm{sgn}(z_2) - \tau_e \end{aligned} \tag{42}$$

where $\hat{\Theta}$ denotes the estimate of Θ_d, and it is updated by

$$\dot{\hat{\Theta}}_i = -\Gamma_i\xi_i^T z_{2i} \tag{43}$$

where Γ_i is a positive real number.

Substituting the control input (42) into (39)

$$\dot{V}_2 = -W + z_2^T\tilde{\Theta}^T\xi + z_2^T w - z_2^T\Lambda\mathrm{sgn}(z_2) \tag{44}$$

where $W = (\Delta\varepsilon_q^T + \Delta\varepsilon_x^T J(q))(\Delta\varepsilon_q + J^T(q)\Delta\varepsilon_x) + z_2^T K_2 z_2$ and $\tilde{\Theta} = \hat{\Theta} - \Theta^*$.

The closed-loop formula of the system is obtained by combining (24) and (40) as

$$M\dot{z}_2 + Cz_2 + \Delta\varepsilon_q + J^T(q)\Delta\varepsilon_x + K_2 z_2 = 0. \tag{45}$$

In order to consider the effect of $\tilde{\Theta}$ on system stability, the total Lyapunov function is designed as

$$V = V_2 + \frac{1}{2}\sum_{i=1}^{n}\tilde{\Theta}_i^T\Gamma_i^{-1}\tilde{\Theta}_i. \tag{46}$$

Taking the time derivative of V and substituting into (44), we have

$$\begin{aligned}\dot{V} = &-W + z_2^T\tilde{\Theta}^T\xi - \sum_{i=1}^{n}\tilde{\Theta}_i\Gamma_i^{-1}\dot{\hat{\Theta}}_i \\ &+ z_2^T w - z_2^T\Lambda\mathrm{sgn}(z_2). \end{aligned} \tag{47}$$

With the updating law (43), we have

$$\dot{V} = -W + z_2^T w - z_2^T\Lambda\mathrm{sgn}(z_2) \tag{48}$$

where the term $\Lambda = \mathrm{diag}[\mathrm{w_{M1}}, \mathrm{w_{M2}}]$ satisfies $|w_i| \le w_{Mi}$; then, we have $z_2^T w - z_2^T\Lambda\mathrm{sgn}(z_2) \le 0$. Therefore, we have following theorem.

Theorem 1: Based on the Lyapunov function in (42) and the update law in (43), the developed adaptive fuzzy-region-based control ensures that the system states in (1) track the desired trajectory, i.e., $x \to x_d$.

Proof: Since V in (46) is positive definite, M and Γ are uniformly positive definite. Therefore, V is bounded owing to $\dot{V} \le 0$, which implies that V_1, z_2, and $\tilde{\theta}$ are bounded according to (36) and (45), and $P_s(q)$ and $P_x(x)$ are bounded because V_1 is bounded. The boundedness of $P_s(q)$ guarantees that $P_E(q)$ and $P_I(q)$ are bounded, and the boundedness of $\Delta\varepsilon_q$ and $\Delta\varepsilon_x$ leads to the boundedness of α_1 according to (33). Therefore, $\dot{q}$ is bounded if $\dot{q}_d$ is bounded according to (24). Since $J(q)$ is a trigonometric function of q, $\dot{x}$ is bounded because $\dot{q}$ and $J(q)$ are bounded. We can conclude that $\dot{z}_2$ is bounded according to (45), so the boundedness of $\ddot{q}$ is guaranteed according to $\dot{z}_2 = \ddot{q} - \dot{\alpha}_1$.

Then, we obtain the derivative of $\dot{V}$ as

$$\begin{aligned}\ddot{V} &= -\dot{W} + \dot{z}_2^T(w - \Lambda\mathrm{sgn}(z_2)) + z_2^T\dot{w} \\ \dot{W} &= 2(\Delta\dot{\varepsilon}_q^T + \Delta\varepsilon_x^T\dot{J}^T(q) + \Delta\dot{\varepsilon}_x^T J(q))(\Delta\varepsilon_q + J^T(q)\Delta\varepsilon_x)) \\ &\quad + 2\dot{z}_2^T K_2 z_2. \end{aligned} \tag{49}$$

According to (49), $\ddot{V}$ is bounded, since α, $\dot{\alpha}$, $\Delta\varepsilon_q$, $\Delta\dot{\varepsilon}_q$, $\Delta\varepsilon_x$, $\Delta\dot{\varepsilon}_x$, z_2, and $\dot{z}_2$ are bounded. Thus, $\dot{V}$ is uniformly continuous;

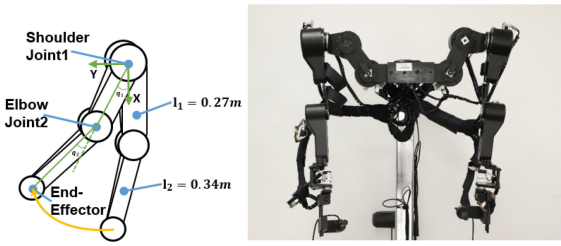

Fig. 6. Exoskeleton robot.

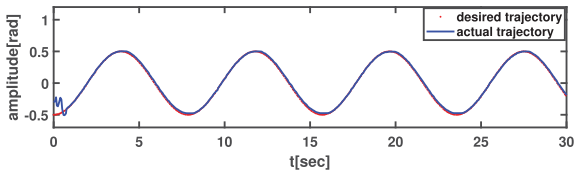

Fig. 7. Joint1's tracking trajectory in joint space.

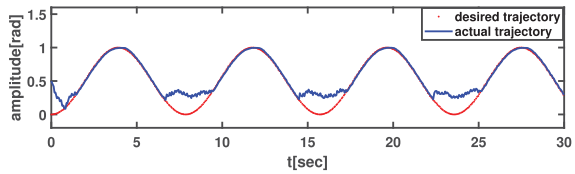

Fig. 8. Joint2's tracking trajectory in joint space.

then, $\dot{V} \to 0$ can be confirmed according to Barbalat's lemma [37]. In other words, we have the following equation:

$$\Delta\varepsilon_q + J^T(q)\Delta\varepsilon_x \to 0. \tag{50}$$

The next is to show that the system is stable in the task-prioritized region but not stable in the singular configurations by contradiction: assuming that the system is in external or internal singular configurations, then $\Delta\varepsilon_q \neq 0$ and $\Delta\varepsilon_x = 0$, which contradicts (50). Therefore, $\Delta\varepsilon_q = 0$ and $\Delta\varepsilon_x = 0$ according to (50); then, $\frac{\partial P_E(x)}{\partial \Delta x} = 0$. From (29), we can have $\frac{\partial f_E(\Delta x)}{\partial \Delta x} = 0$ on the basis of $\frac{\partial P_E(x)}{\partial \Delta x} = 0$, which means $x \to x_d$ as $t \to \infty$. ■

V. Experiment

A. Experimental Setup

Since the robot systems are often modeled as Euler–Lagrange systems, the experiments are performed on the first two joints of the robotic exoskeleton in the Wearable Robotics Laboratory, University of Science and Technology of China, as shown in Fig. 6, to demonstrate the effectiveness of the designed controller. The lengths of the first and the second link are $l_1 = 0.27$ and $l_2 = 0.34$ m, respectively. Two dc motors, Maxon EC90Flat, are used for the exoskeleton robot system as actuators. The Elmo SOL-WHI5/60E01 is used as motor drivers with the CANopen Module. The Jacobian matrix of the robot is given in (7). External and internal singularities occur when $q_2 = 0$ and $q_2 = \pi$, respectively, according to $\det[J(q)] = l_1 l_2 \sin(q_2) = 0$.

In the experiments, the following parameters are selected. The choice of region radius should consider some factors. A larger radius can lead to more effective singularity avoidance, but with a price of more restricted workspace of the system. On the contrary, a small radius often leads to an improved workspace and limited singularity avoidance. In these experiments, external and internal singular regions are defined with $b_E = \pi/12$ in (9) and $b_I = \pi/12$ in (10), respectively. The parameters in (17) and (20) are designed as $N = 2$; the parameters α_s in (15) and α_x in (22) are designed as 0.25 and 0.2, respectively. The parameter of the update law (43) is $\Gamma_i = 0.1$. The control parameter in (42) is $K_2 = [1.5, 1.2]^T$. For fuzzy systems, according to Properties 1 and 2, the six fuzzy sets are labeled as A_1^1, A_1^2, A_1^3, A_4^1, A_1^5, and A_1^6 for each variable x_i, which are characterized by $\mu_{A_i}^l(x_i) = \exp(-(\frac{x_i - \overline{x}_i^l}{\pi/12}))$, and the centers $\overline{x}_i^l$ spaced evenly to span the input space $[-1, 1]$. Membership functions for all variables of fuzzy controller are detailed in Figs. 9 and 10.

The desired trajectory is defined as

$$\begin{cases} q_1 = 0.5\sin(0.8t + \frac{3\pi}{2}) \\ q_2 = 0.5\sin(0.8t + \frac{3\pi}{2}) + 0.5 \end{cases}. \tag{51}$$

The robotic end-effector starts from $(-0.31, 0.48)^T$, where q_2 is near the external singular position. The desired trajectory of the end-effector is a reciprocating curve in the task space. The robotic end-effector starts from the singular region (see the green circle in Fig. 16) and performs a reciprocating curve motion. The end position of reciprocating motion is $(-0.3, 0.54)^T$, where q_2 is also near the external singular region $q_2 = 0$. The experiment demonstrates the performance of the proposed controller when the robotic end-effector starts from singular regions and transits to nonsingular regions and moves from nonsingular regions into singular regions.

B. Experimental Results

Experimental results are shown in Figs. 7–16. From Figs. 7, 8, 11, and 16, the actual trajectories closely tracked the desired trajectory with small error outside singular regions. When the robotic end-effector begins to move in the initial position where external singularity exists, the joint-space region control component $\Delta\varepsilon_q$ is activated and intentionally pushed it into the nonsingular regions. Once the end-effector is away from singularities, the task-space region control component $\Delta\varepsilon_x$ is activated to track the desired trajectory. It should be noted that whenever the robot moves near the end position of the curve where external singularity exists, the control component $\Delta\varepsilon_q$ is activated to push the end-effector to leave the external singularity by applying an opposite torque (see the red curve inside the green circle in Fig. 16).

From Fig. 13, the coefficient β becomes large when end-effector's position is near external singularity and the direction of motion moves toward it, and becomes small when the end-effector is away from external singularity. Whenever effector's position is near external singularity but the direction of motion

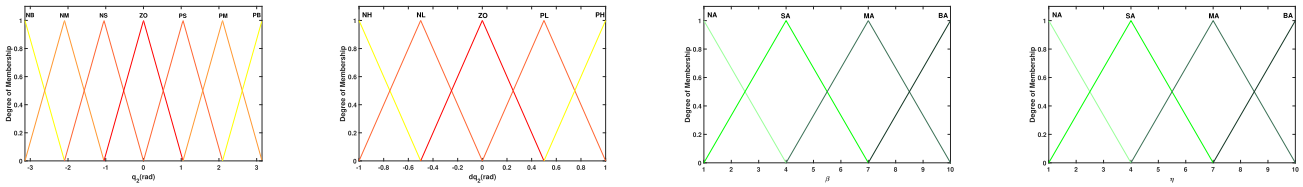

Fig. 9. Membership functions for (a) q_2, (b) $\dot{q}_2$, (c) β, and (d) η.

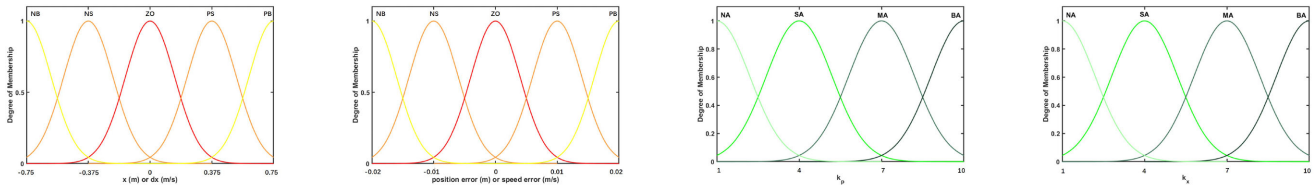

Fig. 10. Membership functions for (a) x or $\dot{x}$, (b) position or speed error, (c) k_p, and (d) k_x.

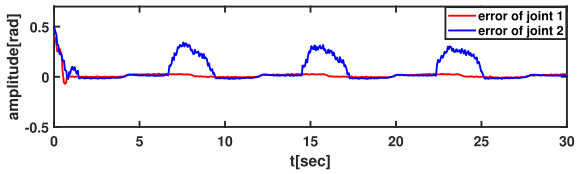

Fig. 11. Error trajectory in joint space.

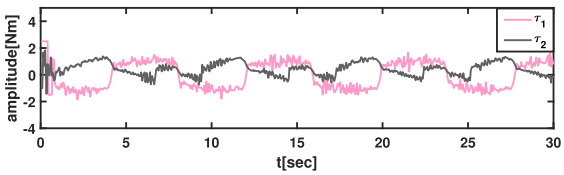

Fig. 12. Torque trajectory in joint space.

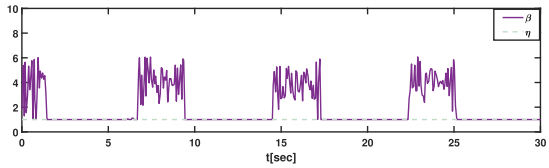

Fig. 13. Coefficient of the potential energy function.

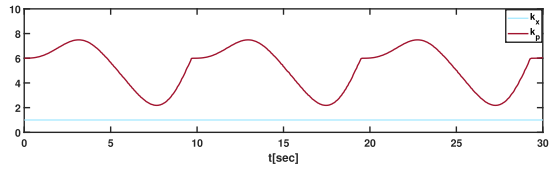

Fig. 14. Coefficient of the potential energy function.

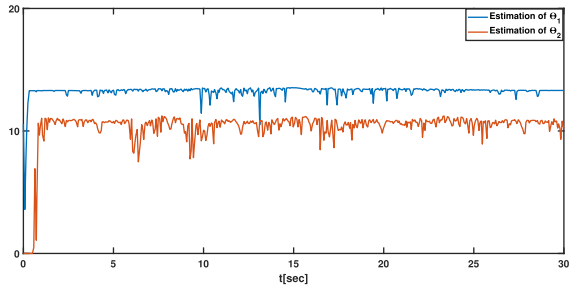

Fig. 15. Estimation of unknown robot dynamics.

deviates from it, the coefficient β decreases, so the control input decreases accordingly. It can save extra effort when robotic exoskeleton avoids the external singularity. Because robotic exoskeleton has a mechanical limit, the experiment does not involve the internal singular region, i.e., $q_2 = \pi$, and the coefficients of the potential energy function η and k_x are always the minimum, i.e., $\eta = 1$ and $k_x = 1$. According to Fig. 14, the coefficient k_p becomes larger to track the desired trajectory more effectively when the position error and the speed error are large. Similarly, when the position error is large but the direction of motion moves toward the desired position, the coefficient k_p decreases a little bit, so the control input of the system decreases accordingly. It can save extra effort when robotic exoskeleton tracks the desired position. The coefficient k_p becomes small when the tracking error is small and reduces to the minimum at the desired position. From Fig. 15, the feedforward fuzzy approximator $\hat{\Theta}$ completed the estimation of the unknown parameters in the robot dynamics within 2 s. Experimental results show that our method has some advantages compared with other singularity-avoidance methods in [28] and [29]. First, our approach dynamically adjusted and optimized gain coefficients of

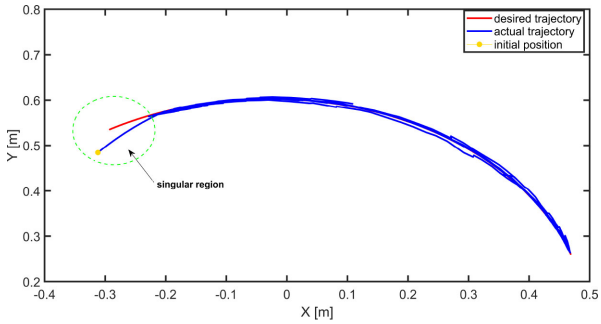

Fig. 16. Tracking trajectory in task space.

the controller by combining the characteristics of the fuzzy system, which can enable smooth transitions of the Euler–Lagrange system from singular regions to nonsingular regions and can also achieve singularity avoidance during the tracking task. Second, singularity avoidance is achieved in both joint space and task space. Third, the use of fuzzy control enhances the robustness of the system in the sense that it does not require accurate system models.

In order to make the proposed controller suitable for various practical scenarios, the controller should hold all of its desired properties during parameter adjustment. If the end-effector is desired to avoid singular regions with more flexibility, the radius of singular regions b_E and b_I and parameters $\beta_{\max}, \eta_{\max},$ and α_s in (27) should be set larger to ensure maximum avoidance of the singularity. However, the choice of parameters $\beta_{\max}, \eta_{\max},$ and α_s should not be too large to cause the system oscillation. The parameters α_x and k_p are fine tuned together to achieve desired trajectory tracking in the task-space region, where short region restoration rise time and smaller steady-state error can be achieved by selecting larger α_x and k_p. Other parameters such as K_2 and Γ_i are also related to the control performance, which should be limited to a small fine-tuning zone. The parameter adaptation gain Γ_i should be tuned from a very small value and should be adjusted when faster parameter adaptation is needed. The choice of K_2 should keep the balance between the maximum output torque of the motor and the tracking performance. The result demonstrates that the robotic exoskeleton can avoid singularity and transits smoothly from singular regions to nonsingular regions.

VI. Conclusion

In this article, an adaptive fuzzy-region-based control method was developed for Euler–Lagrange systems with kinematically singular configurations. Compared with traditional singularity-avoidance methods, our approach can dynamically adjust and optimize gain coefficients of the controller by combining the characteristics of the fuzzy system. Experimental results showed that this method could enable smooth transitions of the Euler–Lagrange system from singular regions to nonsingular regions and was able to achieve singularity avoidance during the tracking task. Rigorous analysis showed that singularity issues could be well handled, and the asymptotic stability of the system was ensured. Future research will pursue advanced approaches to address the singularity issue while ensuring the robustness of the Euler–Lagrange system. In addition, besides the positions and motion direction of the robot, future work will also take into account its acceleration to further improve the system performance. Finally, minimizing control effort based on system parameter adjustment is also a focus of our future research.

References

[1] J. Klotz, S. Obuz, Z. Kan, and W. E. Dixon, "Synchronization of uncertain Euler-Lagrange systems with uncertain time-varying communication delays," *IEEE Trans. Cybern.*, vol. 48, no. 2, pp. 807–817, Feb. 2018.

[2] J. Klotz, Z. Kan, J. M. Shea, E. L. Pasiliao, and W. E. Dixon, "Asymptotic synchronization of leader-follower networks of uncertain Euler-Lagrange systems," *IEEE Trans. Control Netw. Syst.*, vol. 2, no. 2, pp. 174–182, Jun. 2015.

[3] F. Morabito, A. R. Teel, and L. Zaccarian, "Nonlinear antiwindup applied to Euler-Lagrange systems," *IEEE Trans. Robot. Autom.*, vol. 20, no. 3, pp. 526–537, Jun. 2004.

[4] Y. Li, R. Cui, Z. Li, and D. Xu, "Neural network approximation-based near-optimal motion planning with kinodynamic constraints using RRT," *IEEE Trans. Ind. Electron.*, vol. 65, no. 11, pp. 8718–8729, Nov. 2018.

[5] L. Chen, R. Cui, C. Yang, and W. Yan,, "Adaptive neural network control of underactuated surface vessels with guaranteed transient performance: Theory and experimental results," *IEEE Trans. Ind. Electron.*, vol. 67, no. 5, pp. 4024–4035, May 2020

[6] V. Falkenhahn, T. Mahl, A. Hildebrandt, R. Neumann, and O. Sawodny, "Dynamic modeling of bellows-actuated continuum robots using the Euler-Lagrange formalism," *IEEE Trans. Robot.*, vol. 31, no. 6, pp. 1483–1496, Dec. 2015.

[7] H. Xiao, R. Cui, and D. Xu, " A sampling-based Bayesian approach for cooperative multi-agent online search with resource constraints," *IEEE Trans. Cybern.*, vol. 48, no. 6, pp. 1773–1785, Jun. 2018.

[8] H. Cai and J. Huang, "Leader-following consensus of multiple uncertain Euler-Lagrange systems under switching network topology," *Int. J. Gen. Syst.*, vol. 43, nos. 3/4, pp. 294–304, 2014.

[9] Z. Wang, P. Goldsmith, and J. Gu, "Adaptive trajectory tracking control for Euler-Lagrange systems with application to robot manipulators," *Control Intell. Syst.*, vol. 37, pp. 46–56, 2009.

[10] Z. Yang, Y. Shibuya, and P. Qin, "Distributed robust control for synchronised tracking of networked Euler-Lagrange systems," *Int. J. Syst. Sci.*, vol. 46, no. 4, pp. 720–732, 2015.

[11] S. Khoo, L. Xie, and Z. Man, "Robust finite-time consensus tracking algorithm for multirobot systems," *IEEE Trans. Mechatronics*, vol. 14, no. 2, pp. 219–228, Apr. 2009.

[12] F. Chen, G. Feng, L. Liu, and W. Ren, "Distributed average tracking of networked Euler-Lagrange systems," *IEEE Trans. Autom. Control*, vol. 60, no. 2, pp. 547–552, Feb. 2015.

[13] E. Nuno, R. Ortega, L. Basanez, and D. Hill, "Synchronization of networks of nonidentical Euler-Lagrange systems with uncertain parameters and communication delays," *IEEE Trans. Autom. Control*, vol. 56, no. 4, pp. 935–941, Apr. 2011.

[14] R. Spandan and K. Narayan, "Adaptive-robust control of a class of EL systems with parametric variations using artificially delayed input and position feedback," *IEEE Trans. Control Syst. Technol.*, vol. 27, no. 2, pp. 603–615, Mar. 2019.

[15] A. Abdelkader, "Consensus of nonidentical Euler-Lagrange systems under switching directed graphs," *IEEE Trans. Autom. Control*, vol. 64, no. 5, pp. 1415–1421, Jun. 2011.

[16] J. Mei and W. Ren, "Distributed coordinated tracking with a dynamic leader for multiple Euler-Lagrange systems," *IEEE Trans. Autom. Control*, vol. 56, no. 6, pp. 2108–2114, May 2019.

[17] C. P. Bechlioulis and G. A. Rovithakis, "Robust adaptive control of feedback linearizable MIMO nonlinear systems with prescribed performance," *IEEE Trans. Autom. Control*, vol. 53, no. 9, pp. 2090–2099, Oct. 2008.

[18] T. Meng and W. He, "Iterative learning control of a robotic arm experiment platform with input constraint," *IEEE Trans. Ind. Electron.*, vol. 65, no. 1, pp. 664–672, Jan. 2018.

[19] S. Shamik and D. Bhaskar, "Variational approach for singularity-free path-planning of parallel manipulators," *IEEE Trans. Mech. Mach. Theory*, vol. 38, no. 11, pp. 1165–1183, Nov. 2003.

[20] R. Spandan and K. Narayan, "Adaptive-robust time-delay control for a class of uncertain Euler-Lagrange systems," *IEEE Trans. Ind. Electron.*, vol. 64, no. 9, pp. 7109–7119, Sep. 2017.
[21] Y. Nakamura and H. Hanafusa, "Inverse kinematic solutions with singularity robustness for robot manipulator control," *J. Dyn. Syst., Meas. Control*, vol. 108, no. 3, pp. 163–171, 1986.
[22] L. Sciavicco and B. Siciliano, "A solution algorithm to the inverse kinematic problem for redundant manipulators," *IEEE J. Robot. Autom.*, vol. 4, no. 4, pp. 403–410, Aug. 1988.
[23] C. Y. Chung and B. H. Lee, "Torque optimizing control with singularity-robustness for kinematically redundant robots," *J. Intell. Robot. Syst.*, vol. 28, pp. 231–258, 2000.
[24] T. Yoshikawa, "Manipulability of robotic mechanisms," *Int. J. Robot. Res.*, vol. 4, no. 2, pp. 3–9, 1985.
[25] Y. Nakamura, H. Hanafusa, and T. Yoshikawa, "Task-priority based redundancy control of robot manipulators," *Int. J. Robot. Res.*, vol. 6, no. 2, pp. 3–15, 1987.
[26] C. J. Lin, C. R. Lin, S. K. Yu, and C. C. Han, "Singularity avoidance for a redundant robot using fuzzy motion planning," *Appl. Mech. Mater.*, vols. 479–480, pp. 729–736, 2014.
[27] D. Braganza, W. E. Dixon, D. M. Dawson, and B. Xian, "Tracking control for robot manipulators with kinematic and dynamic uncertainty," *Int. J. Robot. Autom.*, vol. 23, no. 2, pp. 117–126, 2008.
[28] C. C. Cheah and X. Li, "Singularity-robust task-space tracking control of robot," in *Proc. IEEE Int. Conf. Robot. Autom.*, 2011, pp. 5819–5824.
[29] X. Li and C. C. Cheah, "Multiple task-space robot control: Sense locally, act globally," in *Proc. IEEE Int. Conf. Robot. Autom.*, 2012, pp. 265–270.
[30] X. Li and C. C. Cheah, "Global task-space adaptive control of robot," *Automatica*, vol. 49, no. 1, pp. 58–69, 2013.
[31] K. Tu and J. Baltes, "Fuzzy potential energy for a map approach to robot navigation," *J. Robot. Auton. Syst.*, vol. 54, no. 7, pp. 574–589, Jul. 2006.
[32] M. A. K. Jaradat, M. H. Garibeh, and E. A. Feilat, "Autonomous mobile robot dynamic motion planning using hybrid fuzzy potential field," *Soft Comput.*, vol. 16, no. 1, pp. 153–164, 2012.
[33] P. Vadakkepat and O. C. Miin, "Fuzzy behavior-based control of mobile robots," *Transitions Fuzzy Syst.*, vol. 12, no. 4, pp. 559–565, 2004.
[34] D. Chwa, "Fuzzy adaptive tracking control of wheeled mobile robots with state-dependent kinematic and dynamic disturbances," *Transitions Fuzzy Syst.*, vol. 20, no. 3, pp. 587–593, 2012.
[35] R. Featherstone, "The calculation of robot dynamics using articulated-body inertias," *Int. J. Robot. Res.*, vol. 2, no. 1, pp. 13–30, 1983.
[36] T. Kazuo, "Stability analysis and design of fuzzy control systems," *Fuzzy Sets Syst.*, vol. 45, no. 2, pp. 135–156, 1992.
[37] J. J. E. Slotine and W. Li, *Applied Nonlinear Control*. Englewood Cliffs, NJ, USA: Prentice-Hall, 1991.

Hongbo Gao received the Ph.D. degree in computer science from Beihang University, Beijing, China, in 2016.

He is currently an Associate Professor with the Department of Automation, School of Information Science and Technology, University of Science and Technology of China, Hefei, China. He has authored or coauthored more than 30 journal papers. He is the co-holder of six patent applications. His current research interests include unmanned system platform and robotics, machine learning, decision support systems, and intelligent driving.

Wei Bi received the B.S. degree in automation from Guangxi University, Nanning, China, in 2018. He is currently working toward the M.S. degree in control engineering with the University of Science and Technology of China, Hefei, China.

His current research interests include human–robot interaction and motion intention recognition.

Xiaoyu Wu received the B.S. degree in automation from Southwest University, Chongqing, China, in 2017. She is currently working toward the M.S. degree in control engineering with the University of Science and Technology of China, Hefei, China.

Her current research interests include human–robot interaction, motion control design, and exoskeleton robotics.

Zhijun Li (Senior Member, IEEE) received the Ph.D. degree in mechatronics from Shanghai Jiao Tong University, Shanghai, China, in 2002.

From 2003 to 2005, he was a Postdoctoral Fellow with the Department of Mechanical Engineering and Intelligent Systems, The University of Electro-Communications, Tokyo, Japan. From 2005 to 2006, he was a Research Fellow with the Department of Electrical and Computer Engineering, National University of Singapore, and Nanyang Technological University, Singapore. Since 2017, he has been a Professor with the Department of Automation, University of Science and Technology of China, Hefei, China, where he has been the Vice Dean of the School of Information Science and Technology since 2019. His current research interests include wearable robotics, teleoperation systems, nonlinear control, and neural network optimization.

Dr. Li has been the Co-Chair of the Technical Committee on Biomechatronics and Biorobotics Systems of the IEEE Systems, Man, and Cybernetics Society and the Technical Committee on Neuro-Robotics Systems of the IEEE Robotics and Automation Society, since 2016. He is an Editor-at-Large for the *Journal of Intelligent and Robotic Systems* and an Associate Editor for several IEEE Transactions.

Zhen Kan received the Ph.D. degree in mechanical engineering from the Department of Mechanical and Aerospace Engineering, University of Florida, Gainesville, FL, USA, in 2011.

He is currently a Professor with the Department of Automation, University of Science and Technology of China, Hefei, China. He was a Postdoctoral Research Fellow with the Air Force Research Laboratory, Eglin Air Force Base, FL, USA, and the University of Florida Research and Engineering Education Facility, Shalimar, FL, from 2012 to 2016. He was an Assistant Professor with the Department of Mechanical Engineering, The University of Iowa, Iowa City, IA, USA. His current research interests include networked robotic systems, Lyapunov-based nonlinear control, graph theory, complex networks, and human-assisted estimation, planning, and decision making.

Dr. Kan is an Associate Editor for the Conference Editorial Board in the IEEE Control Systems Society and technical committees for several internationally recognized scientific and engineering conferences.

Yu Kang (Senior Member, IEEE) received the Dr.Eng. degree in control theory and control engineering from the University of Science and Technology of China, Hefei, China, in 2005.

From 2005 to 2007, he was a Postdoctoral Fellow with the Academy of Mathematics and Systems Science, Chinese Academy of Sciences, Beijing, China. He is currently a Professor with the Department of Automation, the State Key Laboratory of Fire Science, and the Institute of Advanced Technology, University of Science and Technology of China. His current research interests include adaptive/robust control, variable structure control, mobile manipulators, and Markovian jump systems.